

# Practical Compensation Strategy for Accurate Torque Control in Mass-Produced High-speed Traction IPM E-Drives

Ran Cao  
Zhejiang Zero Run Technology Co.,Ltd.  
Hangzhou, China  
Oregon State University  
Corvallis, Oregon 97331, USA  
randcao801@gmail.com

Dakai Hu  
The MathWorks Inc.  
Natick, Massachusetts, USA  
dakaihu@mathworks.com

Yue Cao, Member, IEEE  
School of Electrical Engineering and  
Computer Science  
Oregon State University  
Corvallis, Oregon 97331, USA  
yue.cao@oregonstate.edu

**Abstract**—Accurate torque control of interior permanent magnet (IPM) synchronous machines across the full speed range is the main control goal for EV/HEV traction applications. In this paper, the leading causes for torque inaccuracy in mass-produced IPM drive systems are thoroughly analyzed. Both parameter inconsistency and sensor errors in mass-produced IPMs can lead to errors in Field-Oriented Control (FOC). These FOC-related errors eventually result in the deterioration of high-speed performance. The general relation of torque and output voltage to current angle is deduced mathematically. Then it is used to develop a compensation strategy to achieve the required torque accuracy while maintaining the motor's efficiency in the high-speed region, even under imperfect motor and inverter parameters in the actual commercial products. The method's effectiveness is validated on a 200 kW/15000 rpm industry-grade traction IPM e-drive product.

**Index Terms**—interior permanent magnet machines, accurate torque control, flux-weakening control, DC-link voltage utilization, commercial motor drives

## I. INTRODUCTION

Nowadays interior permanent magnet (IPM) machines play a dominant role in electric drivetrain applications due to their high efficiency and power density, and wide constant-power speed range. The main control goal for high-performance traction IPM machines in EV applications is fast and accurate torque control with high efficiency. Meanwhile, flux-weakening (FW) control is also essential because of the wide speed range and the limited DC-link voltage. In order to achieve these goals, practical control algorithms typically include look-up table (LUT) based open-loop torque control strategies that can address the motor nonlinearity and maintain a fast torque response [1]. Before calibrating the LUT data, characterization tests are often required on the e-motor with paired inverter using a dynamometer setup [2, 3]. Once these characterization tests are done through the pre-determined design of experiments (DoE), multiple torque to current maps that satisfy the accurate torque control and flux-weakening control can be calibrated and stored in the firmware for commercial mass production.

The calibration and LUT based torque control works well if the parameters of mass-produced inverters and motors perfectly match the ones used for calibration. However, the parameter inconsistency issue in both inverters and motors is common in mass-produced applications. On the one hand,

inverters' inherent current sensor errors in both sampling delay and gain introduce current sampling errors. On the other hand, the motor's permanent magnet flux linkage also varies because of the manufacturing process and different thermal conditions. These practical issues inevitably compromise mass production performance with LUT based torque control, especially for the medium to high-speed operation points that are typical for passenger vehicles.

The impact of parameter deviations has two aspects. The first aspect is that the torque accuracy cannot be guaranteed using the pre-determined torque-to-current maps derived from calibration. Improving torque control accuracy for traction IPM drives remains relevant over the years. Methods involving torque feedback control were discussed in [4, 5], whereas the torque accuracy is compromised because of inaccurate torque estimation with incorrect parameters. Papers [1] and [6] proposed a power and motor loss compensation based precise torque control but relied heavily on either calibration or accurate modeling, which faces the same challenge as the LUT based torque control strategy. The second aspect is the high-speed performance deterioration including torque error and voltage saturation issues. Since the reference current trajectory from calibration also serves the purpose of flux-weakening control, the voltage limitation cannot be met because of parameter errors, which means that the current regulation is at risk of losing control. For safety-critical EV applications, additional FW strategies must be adopted as foolproof measures. In light of this, many researchers focused on improving FW control performance. Conventional methods adopt voltage feedback based speed or flux regulation for robust control or high DC bus utilization in response to DC-bus voltage and motor parameter variations [7-10]. However, these methods fail to guarantee torque accuracy while dealing with the voltage saturation issue. In addition, they cannot handle the case in which the DC-link voltage is not fully utilized in the FW region under an imperfect  $d/q$  synchronous reference frame due to parameter variations. The claimed FW strategies cannot be triggered in this scenario. Thus the torque accuracy and low DC-link voltage utilization issues are left unsettled, potentially compromising the e-drive's overall efficiency and maximum torque capacity.

Hence, to improve the IPM e-drive's torque control accuracy and efficiency against the imperfect parameters in actual mass productions, this paper presents a practical compensation strategy to guarantee the torque control

accuracy and DC-link voltage utilization in the high-speed region. In Section II, the practical parameter inconsistency issue in mass-produced IPM e-drive systems and its influence on IPM drive performance are fully explained. In Section III, the general relation of torque and output voltage to current angle is deduced based on the motor model with no approximations. Then a compensation strategy together with LUT based torque control is developed. The proposed method can regulate the output voltage magnitude by either increasing or reducing it, thus maintaining DC-link voltage utilization in the FW region at the expected value even under imperfect motor and inverter parameters. Furthermore, the constraint of DC-link voltage utilization also guarantees the accurate torque response according to the analysis. Finally, in Section IV, simulation with a nonlinear motor model and hardware experimental tests on an industry-grade IPM e-drive system are carried out to verify the effectiveness of the proposed strategy. This compensation method stands out from other strategies, especially for commercial applications, because 1) it ensures that the output voltage is fully utilized and meanwhile guarantees torque accuracy; 2) it is motor model-free and has simple implementation.

## II. ANALYSIS OF IPM MACHINE TORQUE CONTROL ACCURACY

### A. Basic Equations

The steady-state equation of an IPM machine in synchronous  $d/q$  reference frame is given by

$$\begin{cases} \begin{bmatrix} U_d \\ U_q \end{bmatrix} = R_s I_s \begin{bmatrix} \cos\theta \\ \sin\theta \end{bmatrix} + \omega_e I_s \begin{bmatrix} -L_q \sin\theta \\ L_d \cos\theta \end{bmatrix} + \omega_e \begin{bmatrix} 0 \\ \lambda_f \end{bmatrix} \\ T_e = 1.5P_n [\lambda_f I_s \sin\theta + 0.5(L_d - L_q) I_s^2 \sin 2\theta] \end{cases} \quad (1)$$

where  $U_d$  and  $U_q$  are stator voltages,  $I_s$  is stator current magnitude,  $\theta$  is current angle (relative to positive  $d$ -axis),  $R_s$  is stator resistance,  $\omega_e$  is electrical angular speed,  $L_d$  and  $L_q$  are  $d$ - and  $q$ - axis inductances,  $P_n$  is motor pole pair,  $T_e$  is electromagnetic torque, and  $\lambda_f$  is PM flux linkage.

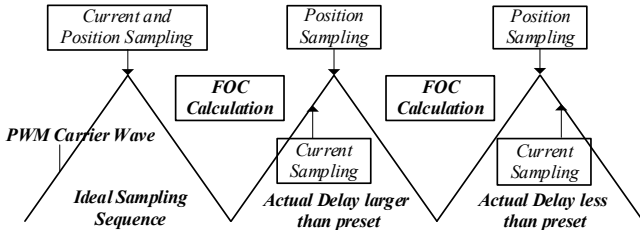


Fig.1 Current sampling sequence with non-ideal hall sensor

### B. Practical Parameter Inconsistencies in Mass-Produced E-drive Applications

According to the torque equation in (1), for mass-produced traction IPM e-drive systems under LUT based control, three main factors can affect torque accuracy: stator current magnitude, variations in motor physical parameters, and accuracy of the  $d/q$  reference frame on which  $\theta$  is depended. Current sampling errors in both gain and delay have a significant impact on the first and third factors. A typical current sampling hardware setup consists of hall sensors and anti-aliasing filters. Previous researches have realized the current sampling issue and proposed several methods to reduce errors [11-13]. The gain error is easy to calibrate and

correct. However, the intrinsic measurement delay of a hall sensor varies in the range of 2-6  $\mu$ s [14, 15].

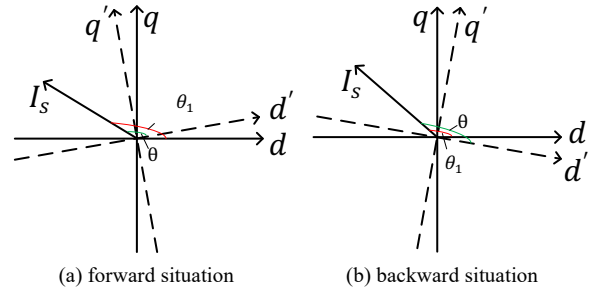


Fig.2 Impact of current sampling delay error on  $dq$  reference frame

The delay inconsistency among mass-produced products introduces a time deviation in the sampling instance between phase currents and rotor position, as shown in Fig. 1. The lagging or leading current sampling results in two separate field orientation errors, as illustrated in Fig. 2 (a) and (b). The former is defined as "forward situation", and the latter is defined as "backward situation".

### C. Impact of Hardware Parameter Inconsistencies on IPM machine Performance

When current control is based on an inaccurate reference frame indicated in Fig.2 (a) and (b), the actual current is  $I_s \angle \theta_1$  instead of  $I_s \angle \theta$  stored in LUTs. The impact of inaccurate current vector caused by reference frame error in FW area is illustrated in Fig.3. The red line is the current limit circle, the black solid and dash lines are voltage limit ellipse, the grey lines are equal torque lines, and the dark blue lines are current vectors under different reference frames. For the operation under an accurate synchronous reference frame,  $\vec{I}_s$  is the current reference vector derived from LUTs, which achieves torque command  $T_{cmd}$ , meanwhile the stator voltage magnitude meets the voltage limit  $U_{s,LMT}$ .  $U_{s,LMT}$  is the maximum allowable output voltage determined by the maximum modulation index (MI), which is defined as  $MI = \sqrt{3}U_s/U_{dc}$ .

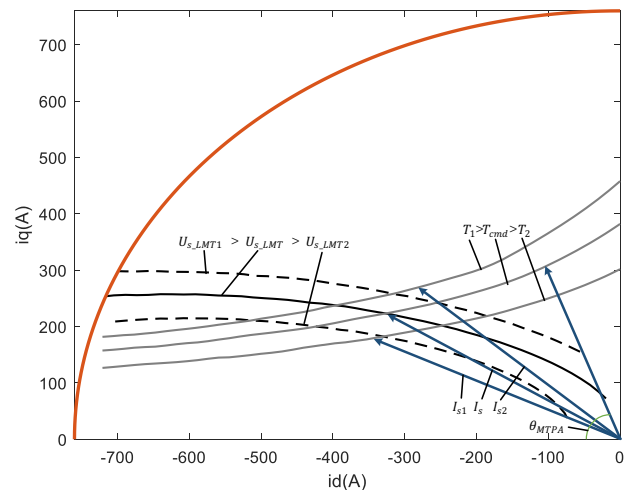


Fig. 3 Impacts of different current vector caused by reference frame error

For the forward situation, the actual stator current vector becomes  $I_{s1}$ . It is evident that the output torque is smaller than  $T_{cmd}$  and the output voltage is smaller than  $U_{s,LMT}$  which means that the DC-bus voltage is not fully utilized.

Since there is no voltage saturation issue in this scenario, the traditional FW methods are not triggered. Therefore, problems of torque error and low DC-bus voltage utilization remain unresolved. For the backward situation, the actual stator current vector becomes  $\vec{I}_{s2}$  which is located outside the voltage-limit ellipse. Thus voltage saturation occurs. The FW control [7-10] will be activated to lower the output voltage through modifying the  $d$ - and  $q$ - axis current reference. After regulation, the new current reference enters the voltage-limit ellipse again, and the output voltage meets the voltage limit. However, the output torque accuracy is not secured since the new current vector might not be the same as  $\vec{I}_s$ . Other factors such as resolver offset error introduced by the manufacturer also lead to a reference frame error. Besides, motor parameters such as PM flux variation caused by the manufacturer or rotor temperature also result in voltage and torque error, as shown in Fig.3.

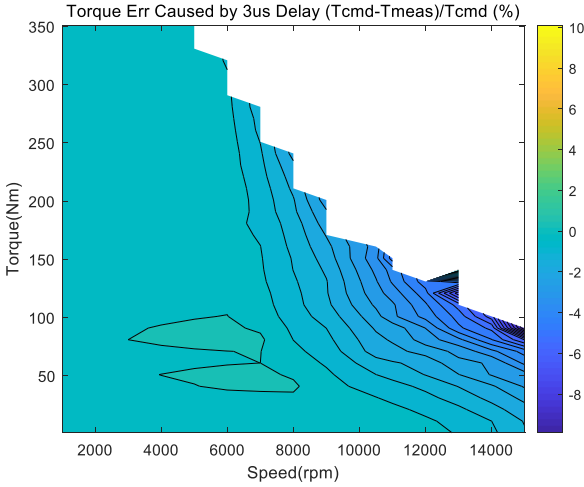


Fig.4 Torque error caused by  $3\mu s$  current measurement delay

Since the reference frame error caused by sampling delays becomes larger with the increase of speed, the drive performances degrade heavily in the high-speed area. For high-power and high-speed IPM machines with large reluctance torque, this degradation gets worse, especially under "forward situation" because torque is extremely sensitive to current angle. Fig.4 shows experimentally tested torque errors caused by a  $3\mu s$  current sampling delay in the full speed range of a 200 kW IPM machine. The average error in the high-speed area is about 5% which is not satisfied enough for a high performance e-drive system.

### III. PROPOSED CONTROL STRATEGY

#### A. General Relation of Torque and Voltage to Motor Phase Current

Defining the square of the output voltage magnitude  $|U_s|$ :

$$|U_s| = \sqrt{U_d^2 + U_q^2} \text{ as } Y, \text{ it can be written as (2) after combing (1).}$$

$$\begin{cases} Y = C + R_s I_s \omega_e [(L_d - L_q) \sin 2\theta + 2\lambda_f \sin \theta] \\ \quad + \omega_e^2 \left[ \frac{L_d^2 - L_q^2}{2} I_s^2 \cos 2\theta + 2L_d I_s \lambda_f \cos \theta \right] \\ C = I_s^2 R_s^2 + \omega_e^2 \left( \frac{L_d^2 + L_q^2}{2} I_s^2 \right) \end{cases} \quad (2)$$

For a fixed  $I_s$  under  $\omega_e$ , the variations of  $d/q$  inductances can be ignored because of the similar level of magnetic saturation imposed by the same current magnitude within a slight angle variation [16]. Then  $C$  can be regarded as a constant term, and  $Y$  is only determined by  $\theta$  from (2). To further evaluate the relation between  $U_s$  and current, the 1st-order differential of  $Y$  with respect to  $\theta$  is derived in

$$\frac{dY}{d\theta} = R_s I_s \omega_e [2(L_d - L_q) \cos 2\theta + 2\lambda_f \cos \theta] + \omega_e^2 [(L_q^2 - L_d^2) I_s^2 \sin 2\theta - 2L_d I_s \lambda_f \sin \theta] \quad (3)$$

$\theta$  is usually within  $(\frac{3\pi}{4}, \pi)$  at a motoring condition in the FW area. Under the constraints of  $R_s > 0, I_s > 0, \omega_e > 0, \lambda_f > 0, L_d > 0, L_q > 0$ , and  $L_d < L_q$ ,  $\frac{dY}{d\theta}$  is always negative. Since  $|U_s|$  is positive, it varies monotonically with  $\theta$  as  $Y$  does. The same conclusion also applies to  $T_e$  by analyzing the differential of torque with respect to the current angle.

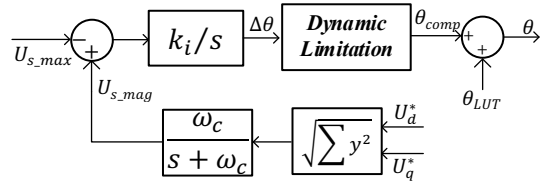


Fig.5 Proposed accurate torque control strategy

According to the above analysis, the current angle error introduced by inaccurate  $d/q$  reference frame error will be reflected in output voltage and torque error. In addition, for a specific current magnitude, only one current angle can ensure that the output voltage equals the voltage limit, which is exactly the objective of FW control. Since output torque also varies monotonically with current angle, the output torque under this current angle will match the value in the 2-D look-up table from calibration. Thus, the torque accuracy is ensured.

#### B. Proposed Angle Compensation Strategy

In light of the previous analysis, a voltage error-based current angle regulator is designed in Fig.5.  $U_d^*$  and  $U_q^*$  are voltage commands calculated by  $d$ - and  $q$ -axis current controllers,  $\theta_{LUT}$  is the initial current reference from LUTs, and  $\theta$  is the final angle of current reference after compensation. A low-pass filter is used to extract the feedback voltage magnitude  $U_{s,mag}$ .  $U_{s,max}$  is the maximum allowable output voltage as  $U_{s,LMT}$  in Section II.

The controller corrects the voltage error between  $U_{s,max}$  and  $U_{s,mag}$  with  $\Delta\theta$  which is either positive or negative, depending on whether the reference frame error is "forward" or "backward". After compensation,  $U_s$  tracks  $U_{s,max}$ , and  $T_e$  equals the torque command. Hence, motor efficiency and torque accuracy are guaranteed.

#### C. Torque Control System with Proposed Strategy

The whole control diagram is depicted in Fig.6, which consists of the basic FOC module, the feedforward part, and the feedback part. In the feedforward part, 2-D LUTs which take torque command  $T_{cmd}$  and electric speed  $\omega_e$  as inputs are applied to generate the initial current reference  $I_{s,mag} \angle \theta_{LUT}$ . At the same time, the MTPA operation angle  $\theta_{MTPA}$  for  $I_{s,mag}$  is identified by a 1-D look-up table, which means the shortest distance from the equal torque line to the

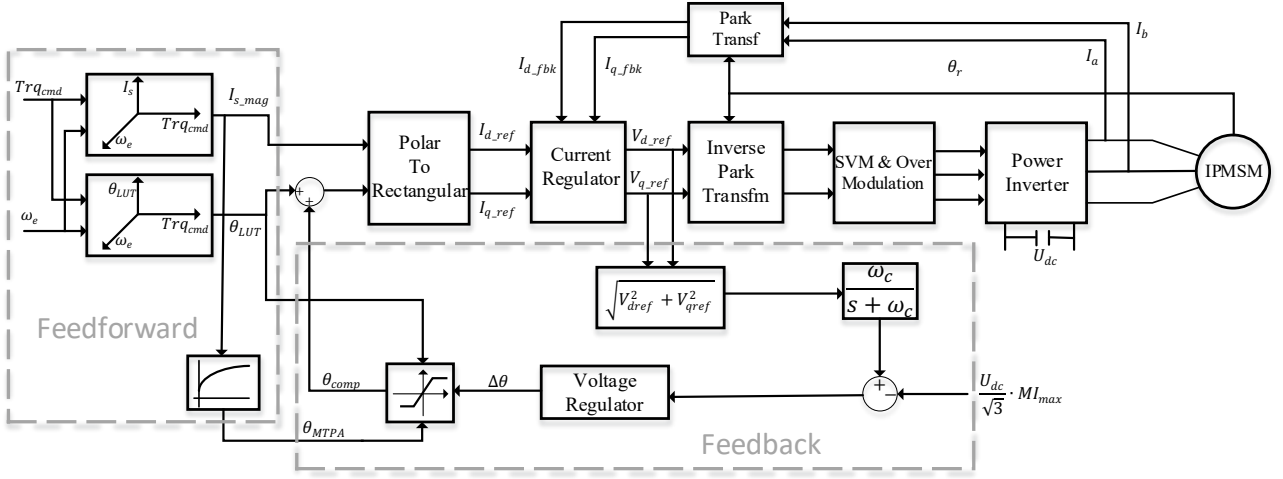


Fig.6 Diagram of torque control system with proposed strategy

origin point in the  $d/q$  coordinate. The final angle for the current reference vector is  $\theta_{LUT}$  plus the compensation from the feedback part.

It is worth noting that  $U_{s\_mag}$  is lower than  $U_{s\_max}$  for the maximum torque per ampere (MTPA) operation. Therefore, a dynamic limitation module is introduced to deactivate the voltage regulation to secure the MTPA operation at the low-speed region. The boundaries of the dynamic limitation module are defined by (4).  $\theta_{MTPA}$  is updated according to real-time torque commands.

$$\begin{cases} \Delta\theta_{min} = \theta_{MTPA} - \theta_{LUT} \\ \Delta\theta_{max} = \pi - \theta_{LUT} \end{cases} \quad (4)$$

For low-speed MTPA operation,  $U_{s\_mag}$  is lower than  $U_{s\_max}$ , so the original  $\Delta\theta$  is negative. At the same time,  $\Delta\theta_{min}$  is 0 (when  $\theta_{MTPA}$  equals  $\theta_{LUT}$ ), so the final  $\theta_{comp}$  is clamped at 0, which means the voltage regulator is deactivated at the low-speed region. Besides, this limitation is also used to reset the integrator in the voltage regulator. For FW operation,  $\Delta\theta_{min}$  is negative ( $\theta_{MTPA} < \theta_{LUT}$ ) and  $\Delta\theta_{max}$  is positive. Therefore, the voltage feedback controller can regulate  $U_{s\_mag}$  in two directions and finally, maintain it at  $U_{s\_max}$ .

#### IV. SIMULATION VERIFICATION

To verify the effectiveness of the proposed strategy, several simulations in MATLAB/Simulink are carried out. In the simulation, the motor plant model is built based on the method in [17] in order to consider nonlinear motor magnetic characteristics. The whole control algorithm is based on Fig.6. As mentioned in Section II, errors in current sampling delay result in inaccurate  $d/q$  synchronous reference frames. The position error is calculated by  $\omega_e \cdot \Delta t$ , where  $\Delta t$  is the sampling delay error. Thus, rotor position is added or subtracted by  $\omega_e \cdot \Delta t$  to emulate current sampling delay error in the simulation.

Fig.7 shows the simulation results with the proposed strategy. The motor ramps to 12000 rpm under 120 Nm.  $\theta_{comp}$  remains at 0 degree before the MI reaches 1.03, followed by a smooth transition between MTPA and FW operations. Rotor positions are offset by  $\pm 1.3$  degree at  $t=0.675s$  and  $t=1.28s$  to emulate  $\pm 6\mu s$  current sampling delays. It is clear in the simulation results that  $\theta_{comp}$  tracks the errors accurately, and the steady state MI and  $T_e$  stay the

same under different angle errors. In addition, the current magnitude remains the same under different errors.

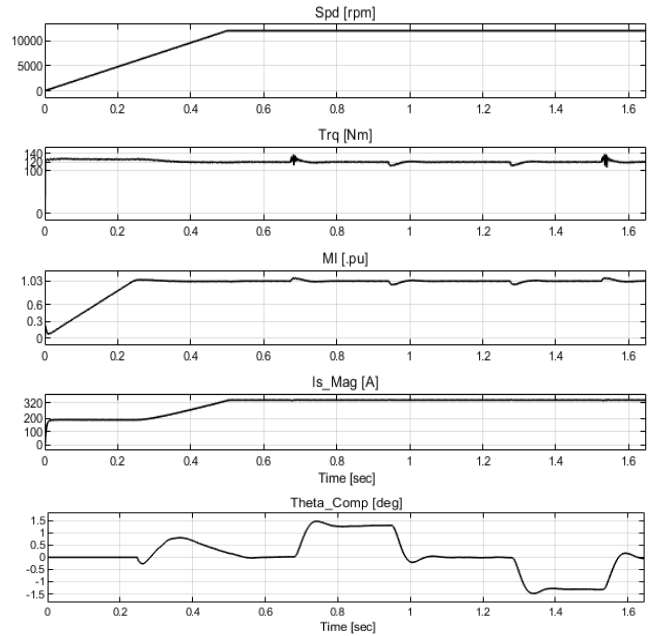


Fig.7 Simulation result with proposed control strategy

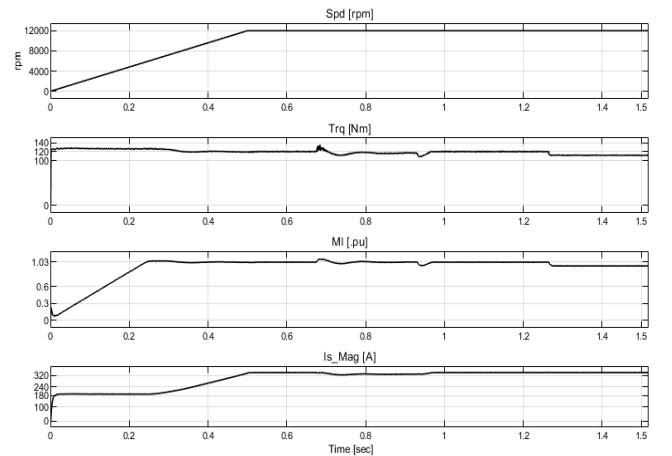


Fig.8 Simulation result with conventional control strategy

As a comparison, Fig.8 is the simulation result based on the classic voltage feedback control strategy. In the "backward" situation, MI maintains at the maximum allowable by the FW control. However, there is an error between the output torque and the torque command. Besides, the current magnitude is also different from the initial LUT value. Under the "forward" condition, MI is 0.96, which is lower than the maximum allowable MI, and the torque loss is approximately 5 Nm.

## V. HARDWARE EXPERIMENTAL VALIDATION

### A. Test System Configuration

The experimental setups are shown in Fig. 9. The tested IPM machine is coupled to a dynamometer through a rigid shaft. The dynamometer controls the motor speed while the IPM machine operates at a torque control mode. The motor torque is measured by the torque transducer (T40B, HBM) on the shaft. Both measurement and control data are uploaded to the central PC workstation through CAN bus and then logged.

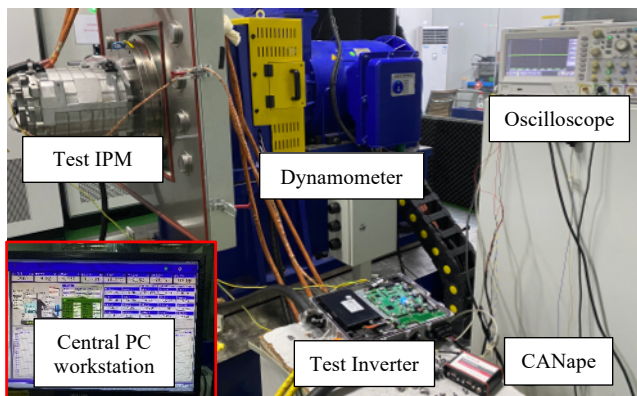


Fig.9 Experimental settings

Parameters of the IPM machine under test are in Table I. The proposed control strategy is implemented in a microcontroller chip (MPC5744p, NXP Semiconductors). The tested e-drive system operates at a torque control mode with LUT based strategy indicated in Fig.6. The torque to current maps derived from experimental calibration are shown in Fig.10 and Fig.11. The DC-link voltage for the test IPM system is maintained at 396V. The switching frequency of the test inverter is 10 kHz, and the current control cycle is 50  $\mu$ s with twice sampling of position/current and PWM duty update per switching cycle. Over-modulation is applied in the system for higher DC-link voltage utilization and high-speed torque capacity. The bandwidth of the complex vector current regulator is 750 Hz, and the maximum allowable steady MI is set at 1.03 (1.0 refers to the maximum output of SVPWM). The integrator coefficient  $K_i$  in the angle compensation module is 4e-5rad/V·s. The current reference generation module and proposed current angle compensator run periodically at 0.5ms intervals.

TABLE I. PARAMETERS OF TEST IPM MACHINE

Variable	Value	Variable	Value
Pole Pairs	3	Peak Speed	15000 rpm
Peak ac current	540 Arms	Maximum torque	360 Nm
Rated line voltage	280 Vrms	Peak Power	200 kW

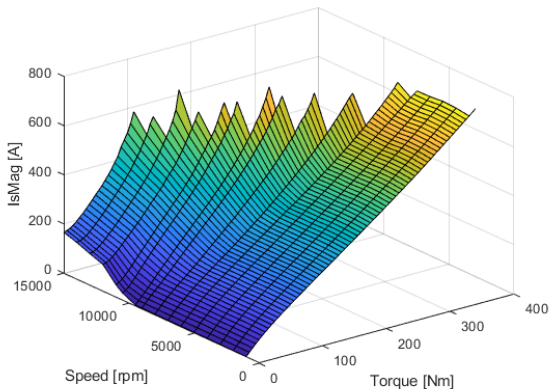


Fig.10 Torque to Current map – Current Magnitude

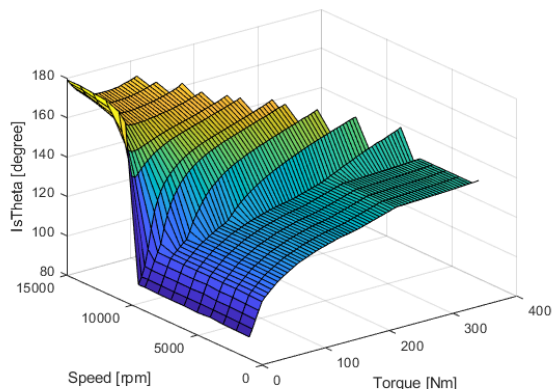


Fig.11 Torque to Current map – Current Angle

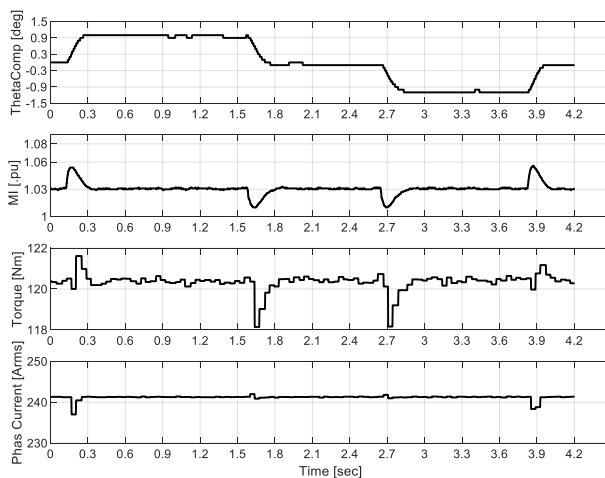


Fig.12 Torque error caused by 3 $\mu$ s current measurement delay

### B. Experiment Results and Discussion

Fig. 12 shows the controller response at 9000 rpm and 120 Nm. At points A and B, step changes of -6 $\mu$ s and 6 $\mu$ s current sampling delay are injected into the control system. As evident in Fig. 12, angle errors are accurately compensated whether the delay error is positive or negative, and the measured torque and MI at steady state are maintained at 120.2 Nm and 1.03, respectively. The phase current also stays the same all the time. The system converges to steady state in less than 200ms under step disturbance. In reality, rather than such a sudden change of error, the error is gradually introduced in the actual system. So the dynamic response with this strategy can meet the requirement of

torque control.

Fig. 13 shows the torque error (%) of the system with 6  $\mu$ s delay, which is less than 1% in the full operation range under the proposed compensation strategy. The torque error is calculated as following: for torque reference under 100 Nm, torque error equals the output torque minus the torque command; for torque reference above 100 Nm, torque error is calculated by  $(T_{meas} - T_{cmd}) * 100 / T_{cmd}$ . The test is conducted with 1000 rpm speed steps from 1000 rpm up to 15000 rpm. At each speed, the torque command is from 0 to the maximum torque with 10 Nm intervals. At each speed's maximum torque capacity point, the actual torque command is sent instead of the multiple of 10 Nm to ensure the torque command is achievable. Each point is tested for 2s to wait for the stable data to be recorded. Similar to the result in Fig.4, the impact of inaccurate reference frame is minor in the low-speed operation area. By introducing the proposed strategy, the torque loss in FW area caused by sampling delay error is greatly reduced. Although the motor thermal condition is carefully monitored during the test, the fluctuation of PM temperature still leads to torque error inevitably because the rotor temperature is hard to be controlled accurately, especially when the motor is being tested continuously for the full operation range. However, due to the nature of the proposed strategy that can guarantee the constant MI at high speed area, the impact of PM temperature variation on the output torque is mitigated. So the overall torque accuracy is still high enough for EV applications.

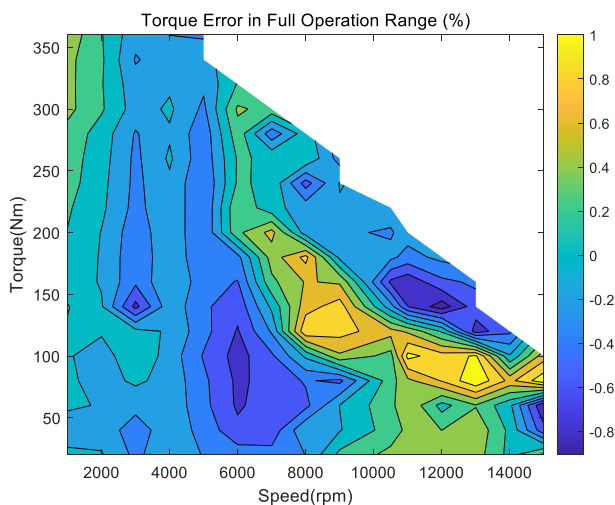


Fig.13 Torque error with proposed control

It is worth pointing out that the current reference is generated by the combination of the feed-forward part and the feedback part, which means that the torque response might not be as fast as the conventional open-loop torque control. However, the dynamic response can be improved by some practical measure. For example, the compensation angle can be stored in the EEPROM of the control hardware for each operation point after first several rounds of operation. Then the saved compensation value can be directly applied later for the same operation points as an initial compensation. Thus the feedback control converges to steady state more quickly, so does the dynamic torque response of the e-drive system.

## VI. CONCLUSION

This paper proposes a voltage feedback based compensation strategy to maintain the torque and efficiency performance of mass-produced commercial traction IPM e-drives. Firstly, the practical issue of torque accuracy caused by parameter inconsistencies both in inverters and motors such as sampling delay variations, is thoroughly analyzed. The connection between torque error and parameter variations is established by the general relation of motor torque and output voltage to current angle. As an improvement of the conventional method, the proposed method involves the voltage feedback based current reference angle compensation on maintaining the MI at maximum allowable value for the entire FW operation region. Thus the DC-link voltage utilization is guaranteed, and the torque accuracy is improved against parameter variations in mass-produced e-drive applications. Besides, a simple but effective dynamic limitation module is used to ensure a smooth transition between MTPA and FW operation. Simulink simulations and hardware experimental results show that the error caused by the current sensor delay and the resolver offset or delay can be eliminated. The performance degradation induced by PM fluctuation can be significantly mitigated. In addition, a practical suggestion for further improving the torque response with this strategy is given for EV applications.

## REFERENCES

- [1] W. Peters, O. Wallscheid, and J. Bocker, "A precise open-loop torque control for an interior permanent magnet synchronous motor (IPMSM) considering iron losses," in *Proc. IECON 38th Annual Conference on IEEE Industrial Electronics Society*, 2012, pp. 2877–2882.
- [2] D. Hu, and L. Xu. "Characterizing the torque look-up table of an IPM machine for automotive application." in *Proc. IEEE Conference and Expo Transportation Electrification Asia-Pacific*, 2014, pp. 1-6.
- [3] K. M. Rahman and S. Hiti, "Identification of Machine Parameters of a Synchronous Motor," *IEEE Transactions on Industry Applications*, vol. 41, no. 2, pp. 557–565, Mar. 2005.
- [4] Bing Cheng and T. R. Tesch, "Torque Feedforward Control Technique for Permanent-Magnet Synchronous Motors," *IEEE Transactions on Industrial Electronics*, vol. 57, no. 3, pp. 969–974, Mar. 2010.
- [5] H. Nakai, H. Ohtani, E. Satoh, and Y. Inaguma, "Development and Testing of the Torque Control for the Permanent-Magnet Synchronous Motor," *IEEE Transactions on Industrial Electronics*, vol. 52, no. 3, pp. 800–806, Jun. 2005.
- [6] W. Huang, Y. Zhang, X. Zhang, and G. Sun, "Accurate Torque Control of Interior Permanent Magnet Synchronous Machine," *IEEE Transactions on Energy Conversion*, vol. 29, no. 1, pp. 29–37, Mar. 2014.
- [7] E. Trancho, et al., "IPMSM torque control strategies based on LUTs and VCT feedback for robust control under machine parameter variations," in *Proc. IECON 42nd Annual Conference of the IEEE Industrial Electronics Society*, 2016, pp. 2833–2838.
- [8] E. Trancho et al., "PM-Assisted Synchronous Reluctance Machine Flux Weakening Control for EV and HEV Applications," *IEEE Transactions on Industrial Electronics*, vol. 65, no. 4, pp. 2986–2995, Apr. 2018.
- [9] Y. Chen et al., "Improved Flux-Weakening Control of IPMSMs Based on Torque Feedforward Technique," *IEEE Transactions on Power Electronics*, vol. 33, no. 12, pp. 10970–10978, Dec. 2018.
- [10] Y. Li, Z. Xia, J. Liang, and A. Emadi, "Flux-Weakening Control of Interior Permanent Magnet Synchronous Motors with Extended DC Link Voltage Utilization and Improved Tracking Performance," in *Proc. IEEE Transportation Electrification Conference & Expo*, 2020, pp. 93–98.
- [11] S. Song, J. Choi and S. Sul, "Current measurements in digitally controlled AC drives," *Industry Applications Magazine, IEEE*, vol. 6, no. 4, pp. 51-62, Jul/Aug 2000.

- [12] F. Briz, D. Diaz-Reigosa, M. W. Degner, P. Garcia, and J. M. Guerrero, "Current sampling and measurement in PWM operated AC drives and power converters," in *Proc. International Power Electronics Conference ECCE ASIA*, 2010, pp. 2753–2760.
- [13] L. Jin, H. Lu, Z. Zhang, and T. M. Rowan, "Phase Delay Analysis of Current Sampling in Inverter-Fed Induction Machines," in *Proc. IEEE Energy Conversion Congress and Exposition 2019*, pp. 4091–4096.
- [14] LEM current sensor HAH3DR 900-S0D datasheet. Available at: [https://www.lem.com/sites/default/files/products\\_datasheets/hah3dr\\_900-s0d\\_public\\_datasheet\\_v1.pdf](https://www.lem.com/sites/default/files/products_datasheets/hah3dr_900-s0d_public_datasheet_v1.pdf)
- [15] Nicera current sensor for automotive datasheet. Available at: [https://www.nicera.co.jp/wordpress/wp-content/uploads/2019/06/DataSheet\\_NCT-LAA.pdf](https://www.nicera.co.jp/wordpress/wp-content/uploads/2019/06/DataSheet_NCT-LAA.pdf)
- [16] B. Stumberger, G. Stumberger, D. Dolinar, A. Hamler, and M. Trlep, "Evaluation of saturation and cross-magnetization effects in interior permanent-magnet synchronous motor," *IEEE Transactions on Industry Applications*, vol. 39, no. 5, pp. 1264–1271, Sep. 2003.
- [17] D. Hu, Y. M. Alsmadi, and L. Xu, "High-Fidelity Nonlinear IPM Modeling Based on Measured Stator Winding Flux Linkage," *IEEE Transactions on Industry Applications*, vol. 51, no. 4, pp. 3012–3019, Jul. 2015.